Published in final edited form as:

Phys Med Biol. 2015 May 7; 60(9): 3441–3457. doi:10.1088/0031-9155/60/9/3441.

Design factors of intravascular dual frequency transducers for super-harmonic contrast imaging and acoustic angiography

Jianguo Ma[1], **K. Heath Martin**[2], **Yang Li**[3], **Paul A. Dayton**[2], **K. Kirk Shung**[3], **Qifa Zhou**[3], and **Xiaoning Jiang**[1]

Jianguo Ma: jma9@ncsu.edu; Xiaoning Jiang: xiiang5@ncsu.edu

[1]Department of Mechanical and Aerospace Engineering, North Carolina State University, Raleigh, NC, 27695, USA

[2]Joint Department of Biomedical Engineering, University of North Carolina and North Carolina State University, Chapel Hill, NC, 27599, USA

[3]Department of Biomedical Engineering, University of Southern California, Los Angeles, CA 90089, USA

Abstract

Imaging of coronary vasa vasorum may lead to assessment of the vulnerable plaque development in diagnosis of atherosclerosis diseases. Dual frequency transducers capable of detection of microbubble super-harmonics have shown promise as a new contrast-enhanced intravascular ultrasound (CE-IVUS) platform with the capability of vasa vasorum imaging. Contrast-to-tissue ratio (CTR) in CE-IVUS imaging can be closely associated with the low frequency transmitter performance. In this paper, transducer designs encompassing different transducer layouts, transmitting frequencies, and transducer materials are compared for optimization of imaging performance. In the layout selection, the stacked configuration showed superior super-harmonic imaging compared with the interleaved configuration. In the transmitter frequency selection, a decrease in frequency from 6.5 MHz to 5 MHz resulted in an increase of CTR from 15 dB to 22 dB when receiving frequency was kept constant at 30 MHz. In the material selection, the dual frequency transducer with the lead magnesium niobate-lead titanate (PMN-PT) 1-3 composite transmitter yielded higher axial resolution compared to single crystal transmitters (70 μm compared to 150 μm pulse length). These comparisons provide guidelines for design of intravascular acoustic angiography transducers.

1. Introduction

Atherosclerosis is a cardiovascular disease, causing 1 death every 40 seconds on average in United States according to the latest Heart Disease and Stroke Statistics (Go *et al.*, 2014). Atherosclerotic plaque rapture is hypothesized to be the majority of secondary cardiovascular events and causes up to 75% of the acute coronary syndromes (Naghavi *et al.*, 2003). However, the evaluation of plaque vulnerability based on measuring coronary intima thickness, degree of stenosis, or other morphological features is ineffective at predicting which plaques will be dangerous in the future if not acted upon (Vallabhajosula and Fuster, 1997). More recently, it has been found that these vulnerable plaques typically express disorganized and excessive vasa vasorum microvessels that supply oxygen and

nutrients to unstable plaques and are linked with atherosclerosis (Carlier *et al.*, 2005; Doyle and Caplice, 2007). Experiment and clinical studies have shown that the presence of angiogenesis and inflammation is a remarkably consistent feature of vulnerable plaques (Shah *et al.*, 2007). Hence, identification of vasa vasorum within plaque bodies is expected to provide an early evaluation of the plaque vulnerability and prediction of the disease.

However, detection of the disorganized vasa vasorum remains challenging due to the low acoustic scattering of blood compared to tissue (Dayton and Rychak., 2007). In order to increase the scattering from the microvessels, ultrasound contrast agents (UCA), e.g. microbubbles, are injected into blood to provide strong acoustic scattering (Frinking *et al.*, 2000; Guo *et al.*, 2014). However, imaging at fundamental frequencies produces low contrast to tissue ratio (CTR) because the scattering from UCA is at comparable level with that from tissue (Klibanov, 1999). Taking the advantage of the highly nonlinear acoustic response of microbubbles compared to tissue, detecting signals at the second harmonic frequency allows for the separation of microbubble signal from tissue signal and increases CTR (Goertz *et al.*, 2006; Bader and Holland, 2013; Wang *et al.*, 2014). Furthermore, it has been shown that super-harmonic imaging occurring at higher harmonics (at the third or greater) has even higher CTR than the images produced using second order harmonics (Bouakaz *et al.*, 2003). When performed with a low frequency transmitter and high frequency receiver, super-harmonic imaging can occur at harmonics of even higher order (5^{th} +) to produce ultrasound images with very high CTR and imaging resolution similar to X-ray angiography in a method referred to as “acoustic angiography” (Gessner *et al.*, 2012; Gessner *et al.*, 2013). Furthermore, both CTR and resolution could be enhanced by in the super-harmonic imaging using triple frequency array with frequency compounding method in the transmission (Danilouchkine *et al.*, 2013).

Another major challenge of vasa vasorum imaging lies in the high attenuation of high frequency ultrasound needed for high resolution detection, which prevents transcutaneous ultrasound probes from being used in coronary vasa vasorum imaging. The diameters of typical vasa vasorum is small and ranges from 161 μm for primary vessels to 68 μm for secondary vessels (Kwon *et al.*, 1998). Intravascular ultrasound (IVUS) imaging may be a solution to this challenge, and has been widely utilized for the characterization of coronary vessel walls (Tobis *et al.*, 1991), morphology of plaques (Jang *et al.*, 2002), and so on (Slager *et al.*, 2000; Jiang *et al.*, 2006; Yuan *et al.*, 2006; Yuan *et al.*, 2008). However, conventional IVUS transducers are not optimized for contrast imaging (Nissen *et al.*, 1991), and therefore are ineffective for vasa vasorum imaging.

We have previously reported a preliminary design of a small aperture, dual frequency (6.5 MHz / 30 MHz) transducer for contrast enhanced intravascular ultrasound (CE-IVUS) imaging (Ma *et al.*, 2013c;Ma *et al.*, 2014a). The low frequency element was used to transmit large amplitude excitatory signals to produce nonlinear response of UCAs while the broadband (10 MHz – 30 MHz) super-harmonic signals were detected by the high frequency receiving element(Ma *et al.*, 2013b). High resolution (< 200 μm) and reasonable CTR (12 dB) was achieved in a tissue mimicking phantom (Ma *et al.*, 2014c).

In this paper, we explore alternatives of the layout designs, transmit frequencies, and transducer materials to provide a guideline for the construction of dual frequency intravascular transducers. Transducers with varying design alternatives were prototyped and tested in a tissue mimicking phantom to evaluate its effect on image quality of CE-IVUS in an effort to optimize parameters for effective vasa vasorum imaging.

2. Materials and Methods

2.1. Layout design

Configurations of the dual frequency transducers could be mainly classified by the relative position of the elements with different frequencies. For a dual frequency transducer, the elements of the two frequencies could be aligned either horizontally (side by side or interleaved) or vertically (stacked), as shown in Figure 1 (Martin *et al.*, 2014). Outer dimensions of IVUS transducers are typically limited by the dimensions of the catheters that house them. In order to be integrated in commercial catheters (Boston Scientific Corp., Natick, MA, USA) typically used for coronary interventions, the width (lateral dimension) of the transducers was limited to 0.6 mm. The length (elevation dimension) could be relatively large in order to provide strong acoustic pressures for nonlinear microbubble oscillations. In addition, it is desirable for both the transmitting and receiving beam to overlap with each other, so that the region generating nonlinear signals coincides with the main lobe of the receive beam. Interleaved and stacked configurations with modifications (Figure 1(a -d)) were compared in order to evaluate their advantages and limitations.

There are several alternatives for the horizontal alignment. One is the ring-shape alignment for piston transducers, usually with the high frequency element in the center and the low frequency element at the edge (Gessner *et al.*, 2013; Cheng *et al.*, 2011). However, the fabrication process is so challenging that no such transducers have been fabricated for IVUS imaging. Another alignment is to alternate the high- and low-frequency elements in one horizontal dimension (Figure 1(a)), which is referred to as a horizontal stack (Ferin *et al.*, 2007) or interleaved configuration (Bouakaz *et al.*, 2004). Advantages of this configuration include low coupling between the elements, and that matching and backing layers could be designed for each frequency so that individual elements could exhibit optimal performance. Because of less coupling in the vibration modes among the elements, the interleaved configuration is preferable if more than two frequencies are needed to have a good frequency coverage (Danilouchkine *et al.*, 2013; Ku *et al.*, 2004). However, interleaved configurations resemble 2-2 composites (Newnham *et al.*, 1978), and the fabrication process is even more complex than single frequency 2-2 composites since thickness mode resonators with different frequencies and differing thickness must be arranged alternately. The fabrication challenge of this increases as transducer dimensions are scaled down making this approach impractical for small, intravascular transducers with multiple frequencies. In the case of one high frequency element and two low frequency elements (Figure 1(a)), the beam of the high frequency and low frequency elements are not well overlapped, which makes it non-ideal for super-harmonic imaging. Transducers with interleaved or stacked layouts were fabricated to demonstrate the performance. Additional, the sensitivity of the transducers with

this configuration is intrinsically reduced because only half of the aperture is active in either transmission or reception (Neer *et al.*, 2010).

If the elements are bonded with one underneath the other (Figure 1(b)), then the arrangement is referred to as a stacked configuration (Neer *et al.*, 2010). If the materials of both layers are high property piezoelectric materials such as PZT or PMN-PT, then there is a high coupling in the vibration between the two layers (Hossack and Auld, 1993). High intensity focused ultrasound (HIFU) used for therapy applications can take advantage of such coupling can generate dual frequency ultrasound to enhance the ablation efficiency (Ma *et al.*, 2013a). In other conditions such as the super-harmonic imaging, however, this frequency coupling effect is not ideal, because it elongate the pulse length and causing low axial resolution. Methods of decoupling the signals include designing a digital filter isolating transmit and receive bands for widely separated signals (Zhou and Hossack, 2002) or an acoustic filter (AF, in Figure 1(c)) (Ma *et al.*, 2014b; Azuma *et al.*, 2010). For the acoustic filter design, input impedance at the acoustic filter layer Z_{in} is

$$Z_{in}=Z_{AF}\frac{Z_{P2}+jZ_{AF}\tan k\ell}{Z_{AF}+jZ_{P2}\tan k\ell} \quad (1)$$

where Z_{AF} and Z_{p2} are the characteristic impedance of the acoustic filter layer and low frequency piezoelectric layer, k is the wave number ($1 / \lambda$) and (img)$\ell$is the thickness of the acoustic filter layer. Acoustic intensity transmission coefficient T_I is

$$T_I=\frac{4Z_{P1}Z_{P2}}{(Z_{P1}+Z_{P2})^2\cos^2(k\ell)+(Z_{AF}+\frac{Z_{P1}Z_{P2}}{Z_{AF}})^2\sin^2(k\ell} \quad (2)$$

where Z_{P1} is the characteristic impedance of the high frequency piezoelectric layer. With a low impedance Z_{AF} and high impedances of Z_{P1} and Z_{P2}, the lowest acoustic intensity transmission happens at quarter wavelength of the acoustic filter. All of the acoustic filters were designed identical because the receiving elements in different transducers were identical, and an identical design of acoustic filter ($1/\lambda$ of receiving wave) meet all the requirements for both transmitting and receiving. Further details of the acoustic filter and its effect on the low frequency wave are reported in a specific paper (Ma *et al.*). Compared to interleaved configurations, stacked transducers are easier to fabricate and offer higher sensitivity and intrinsically confocal (Neer *et al.*, 2010). As a result, the stacked configuration was selected in this dual frequency IVUS transducer design.

For dual frequency transducers used in super-harmonic imaging, the center frequencies of the elements are widely separated, and hence, the beam profiles cannot be ideal for both frequencies if the aperture dimensions of the two elements are identical. If both apertures are large (3 mm in length), then the natural focus of the high frequency beam would be too far away to be useful in IVUS (> 15 mm in this case). However, if the length of both elements of the transducer were small enough to bring the natural focus of the receiving element inside the vessel, then the aperture of the transmitting element would be too small to

generate sufficient pressure to evoke nonlinear microbubble response. In order to generate good beam profiles at both frequencies, the two elements were designed with different aperture sizes (Figure 1(d)).

The final cross-sectional layout of the transducer is shown in Figure 1(e)). The stacked configuration is used with the high frequency reception element in front of the low frequency transmission element. An acoustic filter layer was placed between the two active layers to suppress the high frequency wave propagation while still permitting the low frequency wave to propagate. The aperture of the high frequency element is smaller (about 1/6 in length) than the low frequency element. Transducers were fabricated using previously established methods (Ma *et al.*, 2014c) but the transmitting frequency and materials were altered as discussed in the following sections.

2.2. Frequencies

Working frequencies of the transducers were determined by the super-harmonic imaging requirements. The selection criteria for choosing an appropriate center frequency of the receiving element included having an adequate penetration depth in order to delineate the boundaries of the tunica media while maintaining the ability to detect the fine vessel structures that compose the vasa vasorum. The center frequency of the transmit element was selected by considering element size (which limits lower frequencies since they are too large to operate in arteries) and nonlinear microbubble response when transmit and receive elements have widely separated center frequencies. Previous studies have shown that images produced from nonlinear microbubble response have increased signal to noise ratio (SNR) when using lower transmit frequencies at a high mechanical index (Lindsey *et al.*, 2014a). Because high frequency element is more sensitive to the transducer dimension, the center frequency for the receiving element was defined first and the center frequency of the transmitting element was decided afterwards.

The center frequency of the receive element was designed to penetrate deep enough while maintaining the ability to detect microvessels. Blood vessel walls (∼ 0.5 dB/cm/MHz, < 5 mm thickness) and blood (∼ 0.2 dB/cm/MHz) (Szabo, 2014) contribute to one-way attenuation only since the nonlinear echo is generated by the microbubble and travel to the receiving element. As an example, a nonlinear echo produced by a microbubble at 30 MHz would propagate to the transducer with less than 5 dB loss in a coronary sized vessel. Meanwhile, in order to resolve second order vasa vasorum (∼ 68 μrn) (Kwon *et al.*, 1998), the pulse length of the receiving signal would be similar as this dimension. The wavelength of the 30 MHz ultrasonic wave is about 50 μm in water or tissue, which is good enough for the vasa vasorum imaging if the pulse is consist of a couple of cycles. Based on these considerations, conventional IVUS transducers usually employ a frequency range of 20 – 40 MHz (Qiu *et al.*, 2014). In this paper, the center frequency of the reception element was defined as 30 MHz, which is the same as previous transcutaneous super-harmonic imaging transducer used in a previous study (Gessner *et al.*, 2013).

The center frequency of the transmitting element used for microbubble excitation was determined by maximizing nonlinear microbubble response while considering the space limitations of intravascular catheters. Experiment results showed that microbubbles with

diameters of about 1 μm were excited efficiently with frequencies from 2 to 5 MHz (Doinikov *et al.*, 2009). However, the width of the transducer was decided to be 0.6 mm, and the transducer was designed to work dominantly in thickness vibration mode, which requires the width-to-thickness ratio to be at least 2 (Lerch, 1990). According to this requirement, the thickness of the transmitting active element is at most 0.3 mm, which is associated with a transmitting frequency of 6.5 MHz. However, the 6.5 MHz frequency is slightly higher than the bubble resonant frequency range (2 – 5 MHz) but can still generate SNR that would be detectable (Lindsey *et al.*, 2014b). Additionally, transducers with lower transmit center frequencies (5 MHz) were fabricated to compare image quality as a function of transmitting frequency in IVUS transducers.

2.3. Piezoelectric material

The dual frequency super-harmonic imaging transducers work in relatively low power environments with moderate excitation voltage, short excitation pulses, and low pulse repetition frequency (PRF). In this application condition, piezoelectric materials with high piezoelectric properties are preferable, such as PZT-5H, PMN-PT, so that the transducers could benefit from higher performance without increased risk of being damaged by dielectric breakdown or self-heating.

In comparison with PZT-5H, PMN-0.33PT single crystal exhibits better piezoelectric properties but lower robustness (Table 1) (Park and Shrout, 1997; Rehrig *et al.*, 2003; Zhang *et al.*, 2015). For small aperture intravascular transducers, high dielectric constants are preferable to match the electric impedance to the machine input/output impedance (typically, 50 Ω). In order to obtain high acoustic pressure output (> 1 MPa) and high detecting sensitivity, high piezoelectric strain constant d_{33} and high coupling factor k_t are preferable. Low acoustic impedance is preferable to achieve better transmission efficiency to water or tissue. While the acoustic impedance of both PZT-5H and PMN-PT are high (> 30 MRayl), piezo-composites generally have lower acoustic impedances (∼ 18 MRayl), which may exhibit better transmitting efficiency. The temperature for the safe operation of PMN-PT (< 65 °C, phase transition temperature) is much lower than the PZT-5H (< 350 °C), which is not a serious problem because the transducer operates at low temperatures(body temperature, 37 °C) and at a relatively low power conditions. According to the above considerations and the material properties shown in Table 1, PMN-0.33PT single crystal is a preferable in comparison with PZT-5H.

Because the transducer will be functioning for imaging purposes a short pulse length is preferable since it provides better axial resolution. For this dual frequency super-harmonic imaging transducer, the wavelength of the transmit element is several (4 – 6) times longer than the receiving element. As a result, decreasing the pulse length of the low frequency element would likely be more efficient at improving axial resolution. PMN-PT 1-3 composite possesses a high coupling factor (k_t is close to $k_{33} \sim 0.9$) and relatively low acoustic impedance (∼ 18 MRayl), which is preferred for a shorter impulse response and higher resolution. In addition, the piezoelectric 1-3 composite was designed with little lateral resonance at the working frequency. The lowest lateral resonant frequency f_L in the 1-3 composite material is (Jiang *et al.*, 2006;Jiang *et al.*, 2007b;Jiang *et al.*, 2007a)

$$f_L = \frac{v_L}{2\sqrt{2d_k}} \quad (3)$$

where v_L is the lateral wave velocity and d_k is the kerf width of the composite. The kerf size of composite was well controlled so that the lateral resonant frequency f_L is at least twice of the thickness resonant frequency. This feature is beneficial as the transverse dimension (width) of the IVUS transducer is close to the thickness for the low frequency element. Shorter pulses could be generated from the PMN-PT 1-3 composite because the transverse mode was reduced so that its thickness mode resonance is better than that in PMN-PT single crystal. However, the pressure output efficiency of PMN-PT 1-3 composite is affected by two competing effects: the acoustic wave generation and propagation efficiencies. Low volume fraction ($\sim$ 50%) of active material leads to lower pressure generation while lower acoustic impedance of the composite material causes higher wave transmitting efficiency. In this research, both PMN-PT single crystal (HC Materials Corp., Bolingbrook, IL, USA) and PMN-PT 1-3 composite transmitters were developed and their performances were compared.

2.4. Transducer characterization

Beam profiles of the transducers with interleaved and stacked configurations were mapped with a hydrophone (HNA-0085, Onda Crop., Sunnyvale, CA, USA), using a linear a motion stage controlled by LabVIEW (National Instruments Co., Austin, TX, USA). For the interleaved configuration transducer, the low frequency element was diced in the center, and the high frequency element was placed at the top of the dicing slot (Figure 1(a)). Layouts shown in Figure 1(b) and (c)) were not fabricated because there were foreseen defects in the design, which was solved by the stacked configuration with different apertures and included an acoustic filter (Figure 1(d)) layout. In the transducer characterization, performances of the interleaved configuration (Figure 1(a)) and stacked configuration (Figure 1(d)) were compared. In order to verify that the transmitting beam would overlap with the receiving beam, the sensitivity of the 30 MHz receiving element was also mapped. The propagation of the 30 MHz wave is generally weak, linear and reciprocal, and as a result, the receiving beam profile mapping was estimated by measuring the transmitting beam with the same hydrophone.

The ability to produce large peak negative pressures (PNP) and short pulse length are key design consideration of the transmitting acoustic wave. A large PNP value produces strong nonlinear response of microbubbles and higher CTR while reducing the number of negative pressure peaks would provide higher axial resolution. In the transmit element characterization, the transducers were excited by a function generator (AFG3101, Tektronix Inc., Beaverton, OR, USA) with either one- or two-cycle bursts at 10 V_{pp}. The transmitted wave from each transducer was measured by the same hydrophone (HNA-0085) at 3 mm away from the transducer. The measured pressure values were normalized to unit voltage (1 V) excitation and the performance of the transmission elements were compared and evaluated based on the normalized acoustic pressure output.

Sensitivity and pulse length are important characteristics of the receiving element for high CTR, high resolution imaging. The bandwidth and the sensitivity of the receiving elements were characterized using a pulse-echo method. The transducer was excited by a customized pulser/receiver system (Li *et al.*, 2014) using a 20 V 1-cycle impulse. A steel block was placed in front of the transducer as the reflection target. Envelope of the echo was calculated as the absolute value of the Hilbert transformation on the time domain signal. Sensitivity of the receiving element was defined as the amplitude of the envelope divided by the 20 V amplitude input. Pulse length of the wave was calculated from the normalized envelope with amplitude higher than a threshold (-6 dB or -20 dB, as indicated).

2.5. Contrast imaging

Contrast imaging with these transducers were tested *in vitro* using a tissue mimicking phantom with fully developed speckle from graphite scatterers. Microbubbles consisting of a lipid-shell and perfluoropropane-filled gas core (Streeter *et al.*, 2010) ($\sim 10^8$ microbubbles/mL) were pumped at a speed of 3 mL/h (26.5 mm/s) through acoustically transparent cellulose tubes (200 μm in diameter) embedded in the phantom to mimic the microbubble circulation in vasa vasorum (Figure 2). The transducers were angularly rotated to scan inside an artificial lumen (drilled hole with 4 mm diameter) of the phantom in order to simulate IVUS imaging inside a coronary vessel. Pulse lengths measured during imaging was defined as the time duration in which the amplitude of the enveloped signal was -6 dB relative to the peak value.

A customized dual channel contrast imaging system (Li *et al.*, 2014) was used to excite the transducers and to acquire the signal. The system was controlled by Xilinx Virtex-6 FPGA (Xilinx Inc., San Jose, CA). The transmission excitation was adjustable as 1 – 33 MHz and 20 – 100 V and the reception was sampled up to 200 MS/s. A synchronized 3-dimensional (3D) motion stage and a stepper motor (400 steps/rev) were used to position and rotate the transducer for imaging.

3. Results

3.1. Transducer prototypes

Multiple transducers were fabricated and their performance was evaluated with acoustic characterization and super-harmonic imaging. The center frequencies of the transmitting elements of the transducers were either 6.5 or 5 MHz, while the reception frequency of all three transducers was 30 MHz. The 6.5 MHz transducers were fabricated with PMN-PT single crystals and the 5 MHz transducers were fabricated with both PMN-PT single crystal and 1-3 composite. At least 5 transducers were fabricated in each category. All transducers were identical in aperture (3 mm × 0.6 mm) and similar in thickness (0.3 – 0.45 mm). All the transducers were small enough to be mounted onto 20 gauge hypodermic needles or inside commercial percutaneous intervention catheter housings (Boston Scientific Corp., Natick, MA, USA) (Figure 3).

3.2. Acoustic characterization

3.2.1. Beam map—Transducers with interleaved configuration and stacked configuration were fabricated and their transmitting beam profiles were first mapped to verify that they overlapped with the peak sensitivity of the receiving beam. In the interleaved configuration, there is no piezoelectric material for transmitting at the center of the transducer (the position of the receiving element) and as a consequence, the pressure was lower at the center (Figure 4(b)). However, since the receiving element was designed for good lateral resolution (-3 dB beamwidth: < 0.4 mm), the region that the transducer is sensitive to receiving signal was outside of the peak pressure regions of the transmit beam profile when using an interleaved configuration (Figure 4(a)). Consequently, microbubbles inside the sensitive region of the receiving beam could not be sufficiently excited by the low frequency wave because of non-overlapping beams. The transducer prototypes with interleaved configuration was unable to detect any super-harmonics generated from microbubbles in preliminary experiments. On the contrary, the stacked configuration has piezoelectric material for transmitting placed underneath the receiving element with an acoustic filter layer between the two active layers (Figure 1(d)). As a result, the transmitting beam of stacked transducers was relatively uniform and without a drop of high pressure near the center of the transducer where the receiving element was most sensitive (Figure 4(c)). Further analysis of optimized transducer design excluded the use of the interleaved layout due to its inability to simultaneously generate and detect nonlinear microbubble responses. All remaining analysis sections considered transducers fabricated with the stacked configuration (Figure 1(e)).

3.2.2. Transmitting waveform—Transmission characteristics of the transducers were measured using a hydrophone by applying either a one- or two-cycle wave excitation to the transmitting element. Measured pressures were normalized to the input voltage amplitude applied to the element and plotted (Figure 5).

The normalized pressure value of each transducer that corresponds to 1 V excitation is marked by the horizontal dashed line in Figure 5 in order to facilitate PNP comparisons. The 6.5 MHz transmitter generated relatively higher pressure at the same voltage input (Figure 5, left), primarily for two reasons. First, while the same voltage level was applied, the electric field within the 6.5 MHz transmitter was higher because of the smaller gap distance between electrodes of the higher frequency transmitter. Second, the 6.5 MHz transmitter had reduced lateral mode coupling compared to the 5 MHz transducers since the width-to-thickness ratio was higher (Lerch, 1990). If the frequency was lowered directly by increasing the thickness of the PMN-PT single crystal, then the width-to-thickness ratio is also lowered and the element will split the transduction energy between the transverse and thickness vibration modes which operate at different center frequencies, broadening the transducers bandwidth. In that case, the thickness mode resonance would be weakened and the pressure output was measured to be lower (Figure 5, middle). In order to suppress the transverse vibration mode, the active material could be replaced by PMN-PT 1-3 composite. The pressure output of the 5 MHz PMN-PT 1-3 composite transmitter (Figure 5, right) was slightly higher than that of single crystal although the volume fraction of active piezoelectric material is much less (~ 50% vs 100%).

Pulse length (marked with vertical dashed line in Figure 5) of the acoustic transmitting wave was defined as the time duration within which the negative pressure was at least -6 dB relative to the PNP. Moderate acoustic pressures (∼ 1 MPa) induced detectable super-harmonics from microbubbles while low pressures caused little harmonic response. The 6.5 MHz single crystal transmitter had almost no transverse resonance components (∼ 1.5 MHz), and the pulse length was short with 2 pronounced negative peaks (≥ -6 dB) at the 1-cycle excitation and 3 pronounced negative peaks at the 2-cycle excitation. However, the 5 MHz single crystal transmitter had the longest pulse length with multiple negative peaks even at the 1-cycle excitation. When the material was replaced with 1-3 composite, the transverse vibration mode was largely suppressed and the pulse length became shorter with 1 pronounced negative peak at the 1-cycle excitation and 2 pronounced negative peaks at the 2-cycle excitation. The transmitters made with PMN-PT 1-3 composite were the only ones that exhibited single negative peak waveforms while all PMN-PT single crystal transmitters had noticeable ringdown that generated multiple pronounced negative peaks that may significantly reduce the axial resolution capability of the system.

In summary, the 6.5 MHz transmitter generated the highest pressure output for a given voltage amplitude while the 1-3 composite transmitter generated the shortest pulse length with a single negative peak. The tradeoff between the high pressure of the 6.5 MHz crystal transducer and the short pulse length from the 5 MHz composite transducer can be used to tailor transducer design to adapt to the environment being imaged. The normalized pressure efficiency from the composite material was about half of the 6.5 MHz crystal, which is not dramatically low and can be compromised by supplying higher voltages. Applying 100 V to the composite would generate about 1 MPa of peak negative pressure, which is sufficient for super-harmonic imaging of contrast agents. Additionally, the pulse length of the 6.5 MHz crystal transducer is not short enough and contains multiple cycles with high rarefractional pressures which is undesirable for imaging since it can cause multiple axial responses that would ultimately reduce spatial resolution of the image. Taking these two considerations into account, the 5 MHz composite transmission transducers are expected to be more suitable for a high contrast, high resolution imaging.

3.2.3. Pulse-echo of the receiving element—The 30 MHz reception element of these groups were designed with identical parameters although there were slight variations due to fabrication inconsistency. Typically, a reception element showed high sensitivity (-27 dB loop sensitivity) and short pulse (48.8 μm at -6 dB and 86.0 μm at -20 dB) in pulse-echo response (Figure 6). The -6 dB fractional bandwidth was 46% with the pass band covering from 22.9 MHz to 36.6 MHz which covers the 4th to 7th harmonics of the 5 MHz transmission center frequency. The aliasing echo (Ma *et al.*, 2014b) of the receiving wave was suppressed to 23.7 dB compared to the primary echo.

3.3. Contrast imaging in phantom

The frequency dependence of the CTR was investigated by comparing the imaging results *in vitro* using the transducers with 6.5 MHz and 5 MHz transmitters made of PMN-PT single crystal. For an effective frequency comparison, relatively narrow bandwidth excitations are preferable to differentiate each frequency response. According to the transmitting waveform

measurements (Figure 5), short monotone bursts composed of 2-cycles at the center frequency of each transmit element were used to excite the transducers for comparison. The amplitude of the excitatory signal was adjusted to obtain 1 MPa PNP, a typical value generates nonlinear response from microbubbles consistently without complete destruction of them (Lindsey *et al*., 2014b; Radhakrishnan *et al*., 2013). In the super-harmonic imaging tests, the dual frequency transducer with the 5 MHz crystal transmitter generated images with higher CTR (21.6±3.0 dB, Figure 7(b)) than the one with the 6.5 MHz crystal transmitter (15.4±1.5 dB, Figure 7(a)). The result comparison is concluded in Table 2. There are mainly two causes. One reason was that 5 MHz was closer to the microbubble resonance and transmitted wave was more efficient at generating the nonlinear response of the microbubbles (Doinikov *et al.*, 2009). Another explanation would be that the harmonics being detected at 30 MHz when transmitting with the 5 MHz element are of a higher order (4.6-7.3 times f_c) than the harmonics generated from the 6.5 MHz transmit frequency (3.5-5.6 timesf_c). Other studies have indicated that higher order harmonic energy generated from tissue is lower than that produced by microbubbles (Bouakaz *et al.*, 2002). The 5 MHz transmitter produced better CTR than the 6.5 MHz transmitter in higher order super-harmonic imaging of contrast agents.

The pulse length of the transmitting wave is likely to be the main cause for the change in axial resolution of these two phantom images, and it appears that a single negative peak is preferable for the microbubble excitation. The 6.5 MHz single crystal transducer could not achieve resolutions higher than 150 μm because of multiple negative peaks in the transmission even if 1-cycle excitation was used. In the image, the diameter of the cellulose tube carrying microbubbles was measured to be larger than the actual diameter (Figure 8(a)). Similarly, because of long pulse length in the transmission, the measured diameter of from transducers with 5 MHz single crystal transmitter is also larger than the actual diameter of the tube (Figure 8(b)). In comparison, transducers with the 1-3 composite transmitter under 1-cycle excitation generated very short pulses (single peak) and the measured diameter of the tube in the test was almost the same as the actual value (Figure 8(c)). The -12 dB pulse length was decided on brightest spot with peak value of 0 dB (marked with yellow arrow). Other spots are darker, probably due to less sensitive microbubble sizes, deviation from the receiver's most sensitive bean, etc. Some spots appeared to be shorter because they were not -12 dB pulse length, while some appeared to be longer very likely because of the existence of multiple microbubbles. Considering these effects, the brightest spot width was determined to be the pulse length of the microbubble response, which was about 70 μm at -12 dB, suggesting the possibility of the transducers for high resolution acoustic angiography of the second order vasa vasorum.

No lateral information is illustrated in Figure 8 because lateral resolution is neither the width of the whole bright area, nor the width of each white spot. The microbubble tube was not parallel to the transducer, so the bright area can be wide due to the angle of the tube. Each bright spot is not the lateral resolution because each microbubble can hardly be detected twice. The PRF of the imaging was about 100 Hz, and the bubbles flow speed was about 26.5 mm/s, meaning that the microbubbles travelled about 265 μm in each imaging interval. Considering the narrow beam of the receiver (≤ ± 0.2 mm at -6 dB), if one microbubble is at

the center of the beam in one excitation, it would be out of the beam in the next one. As a result, the bright spots came from different bubbles even if they look close to each other in the lateral dimension.

4. Conclusion

In this paper, dual frequency intravascular ultrasound transducers were designed for vasa vasorum imaging to estimate the vulnerability of coronary plaques. Design alternatives were studies and compared for optimization of image quality by adjusting transducer layout, transmitting and receiving frequencies, and the transducer materials.

Transducers with interleaved layout and stacked configuration were fabricated and characterized by beam mapping. The transducers designed with the interleaved configuration had non-overlapping transmit and receive beams and therefore could not detect super-harmonic signal from microbubbles. On the contrary, the specially designed stacked configuration with an acoustic filter layer and different transmitting/receiving apertures successfully generated uniform transmit pressure fields, which were able to generate detectable nonlinearity of microbubbles at the sensitive area of the receiving element. Therefore, the stacked configuration is more favorable in this dual frequency intravascular transducer design for acoustic angiography.

The transducer frequencies were designed specifically for intravascular vasa vasorum imaging. The receiving element was designed to have a high center frequency since the major concern is to identify fine vessel structures at a shallow depth of a few millimeters (Gessner *et al.*, 2013). The transmitting element was designed to properly excite microbubbles to produce high order nonlinear harmonics. The thickness mode resonator having a center frequency of 6.5 MHz was not very effective at performing nonlinear excitation. The CTR was increased from 15 dB to 22 dB when the transmitting frequency was decreased from 6.5 MHz to 5 MHz. However, unintentional transverse vibration modes were introduced by increasing the thickness of the transmitting element in order to have a lower center frequency and this caused reduced pressure outputs and increased pulse lengths that would degrade image quality. The transverse vibration problem was solved by replacing the PMN-PT transmitting material from a single crystal to a 1-3 composite.

The PMN-PT 1-3 composite transmitters generated much shorter pulses than the PMN-PT single crystal ones. In the PMN-PT 1-3 composite, transverse vibrations at frequencies near the thickness mode resonance were suppressed intrinsically by the periodic structure of the composite allowing filling material to mechanically decouple transverse wave propagation. Additionally, the characteristic acoustic impedance of PMN-PT 1-3 composite (∼18 MRayl) is much lower than that of its single crystal counterpart (∼37 MRayl). Incorporating composites into the design allowed broader bandwidth to be achieved which dramatically reduced the pulse length of the transmitting wave. In super-harmonic imaging with a single crystal transmitter, the detected diameter of the cellulose tube was larger than the actual diameter due to reduced axial resolution caused by increased pulse length of the transmitter. In comparison, measurements of the same micro-tube using the 1 -3 composite transmitter were much closer to the actual diameter of the cellulose tube with individual microbubbles

being detected at a length of 70 μm in the image. These short pulses would aid in creating a very high resolution imaging of tiny vasa vasorum using contrast agents in IVUS.

In conclusion, this paper provided details of the design alternatives and the optimal choices on dual frequency intravascular transducers that are designed for vasa vasorum angiography using higher order super-harmonic imaging approaches. The choices and design methods are expected to be advisable to other super-harmonic imaging transducers as well.

Acknowledgments

The authors would like to acknowledge the financial support from NIH under the grants R01EB015508, R01CA170665, and P41EB02182.

References

Azuma T, Ogihara M, Kubota J, Sasaki A, Umemura Si, Furuhata H. Dual-frequency ultrasound imaging and therapeutic bilaminar array using frequency selective isolation layer. IEEE Trans Ultrason Ferroelectr Freq Control. 2010; 57:1211–24. [PubMed: 20442033]

Bader KB, Holland CK. Gauging the likelihood of stable cavitation from ultrasound contrast agents. Phys Med Biol. 2013; 58:127. [PubMed: 23221109]

Bouakaz A, Frigstad S, Ten Cate FJ, de Jong N. Improved contrast to tissue ratio at higher harmonics. Ultrasonics. 2002; 40:575–8. [PubMed: 12160004]

Bouakaz A, Krenning BJ, Vletter WB, Cate FJT, Jong ND. Contrast superharmonic imaging: A feasibility study. Ultrasound Med Biol. 2003; 29:547–53. [PubMed: 12749924]

Bouakaz A, ten Cate F, de Jong N. A new ultrasonic transducer for improved contrast nonlinear imaging. Phys Med Biol. 2004; 49:3515. [PubMed: 15446784]

Carlier S, Kakadiaris Ia, Dib N, Vavuranakis M, O'Malley SM, Gul K, Hartley CJ, Metcalfe R, Mehran R, Stefanadis C, Falk E, Stone G, Leon M, Naghavi M. Vasa vasorum imaging: a new window to the clinical detection of vulnerable atherosclerotic plaques. Curr Atheroscler Rep. 2005; 7:164–9. [PubMed: 15727733]

Cheng CH, Shen CC, Yeh CK. Dual-frequency chirp imaging for contrast detection. Phys Med Biol. 2011; 56:2767. [PubMed: 21464533]

Danilouchkine MG, Van Neer PL, Verweij M, Matte G, Vletter W, Van Der Steen A, De Jong. Single pulse frequency compounding protocol for superharmonic imaging. Phys Med Biol. 2013; 58:4791. [PubMed: 23787259]

Dayton PA, Rychak JJ. Molecular ultrasound imaging using microbubble contrast agents. Front Biosci. 2007; 12:5124–42. [PubMed: 17569635]

Doinikov AA, Haac JF, Dayton PA. Resonance frequencies of lipid-shelled microbubbles in the regime of nonlinear oscillations. Ultrasonics. 2009; 49:263–8. [PubMed: 18977009]

Doyle B, Caplice N. Plaque neovascularization and antiangiogenic therapy for atherosclerosis. Journal of the American College of Cardiology. 2007; 49:2073–80. [PubMed: 17531655]

Ferin G, Legros M, Felix N, Notard C, Ratsimandresey L. Ultra-Wide Bandwidth Array for New Imaging Modalities. 2007 IEEE Int Ultrason Symp (IUS). 2007:204–7.

Frinking PJA, Bouakaz A, Kirkhorn J, Cate FJT, Jong N. Ultrasound contrast imaging: current and new potential methods. Ultrasound Med Biol. 2000; 26:965–75. [PubMed: 10996696]

Gessner RC, Aylward SR, Dayton PA. Mapping microvasculature with acoustic angiography yields quantifiable differences between healthy and tumor-bearing tissue volumes in a rodent model. Radiology. 2012; 264:733–40. [PubMed: 22771882]

Gessner RC, Frederick CB, Foster FS, Dayton PA. Acoustic angiography: a new imaging modality for assessing microvasculature architecture. Int J Biomed Imaging. 2013; 2013:936593. [PubMed: 23997762]

Go AS, Mozaffarian D, Roger VL, Benjamin EJ, Berry JD, Blaha MJ, Dai S, Ford ES, Fox CS, Franco S. Heart disease and stroke statistics--2014 update: a report from the American Heart Association. Circulation. 2014; 129:e28. [PubMed: 24352519]

Goertz DE, Frijlink ME, Tempel D, van Damme LC, Krams R, Schaar JA, Folkert J, Serruys PW, Jong ND, van der Steen AF. Contrast harmonic intravascular ultrasound: a feasibility study for vasa vasorum imaging. Invest Radiol. 2006; 41:631–8. [PubMed: 16829746]

Guo G, Lu L, Yin L, Tu J, Guo X, Wu J, Xu D, Zhang D. Mechanical and dynamic characteristics of encapsulated microbubbles coupled by magnetic nanoparticles as multifunctional imaging and drug delivery agents. Phys Med Biol. 2014; 59:6729. [PubMed: 25327566]

Hossack JA, Auld BA. Improving the characteristics of a transducer using multiple piezoelectric layers. IEEE Trans Ultrason Ferroelectr Freq Control. 1993; 40:131–9. [PubMed: 18263166]

Jang IK, Bouma BE, Kang DH, Park SJ, Park SW, Seung KB, Choi KB, Shishkov M, Schlendorf K, Pomerantsev E. Visualization of coronary atherosclerotic plaques in patients using optical coherence tomography: comparison with intravascular ultrasound. Journal of the American College of Cardiology. 2002; 39:604–9. [PubMed: 11849858]

Jiang X, Snook K, Hackenberger WS, Geng X. Single crystal piezoelectric composites for advanced NDT ultrasound. The 14th Int Symp Smart Struct Mat & Nondestruct Eval Health Monitor. 2007a: 65310F–8.

Jiang X, Snook K, Hackengerber W, Yuan J, Cheng A, Schafer M, Geng X. 4F-5 PC-MUT Arrays for Ophthalmologic Ultrasound. 2007 IEEE Int Ultrason Symp (IUS). 2007b:309–12.

Jiang X, Yuan JR, Cheng A, Snook K, Cao P, Rehrig P, Hackenberger W, Lavalelle G, Geng X, Shrout T. 5I-1 Microfabrication of Piezoelectric Composite Ultrasound Transducers (PC-MUT). 2006 IEEE Int Ultrason Symp (IUS). 2006:922–5.

Klibanov AL. Targeted delivery of gas-filled microspheres, contrast agents for ultrasound imaging. Adv Drug Deliver Rev. 1999; 37:139–57.

Ku G, Wang X, Stoica G, Wang L. Multiple-bandwidth photoacoustic tomography. Phys Med Biol. 2004; 49:1329. [PubMed: 15128208]

Kwon HM, Sangiorgi G, Ritman EL, McKenna C, Holmes DR Jr, Schwartz RS, Lerman A. Enhanced coronary vasa vasorum neovascularization in experimental hypercholesterolemia. J Clin Invest. 1998; 101:1551. [PubMed: 9541483]

Lerch R. Simulation of piezoelectric devices by two-and three-dimensional finite elements. IEEE Trans Ultrason Ferroelectr Freq Control. 1990; 37:233–47. [PubMed: 18285037]

Li Y, Ma J, Martin KH, Choi H, Dayton PA, Jiang X, Shung KK, Zhou Q. A configurable dual-frequency transmit/receive system for acoustic angiography imaging. 2014 IEEE Int Ultrason Symp (IUS). 2014; 7:31–3.

Lindsey BD, Rojas JD, Martin KH, Shelton SE, Dayton PA. Acoustic characterization of contrast-to-tissue ratio and axial resolution for dual-frequency contrast-specific acoustic angiography imaging. IEEE Trans Ultrason Ferroelectr Freq Control. 2014a; 61:1668–87. [PubMed: 25265176]

Lindsey BD, Rojas JD, Martin KH, Shelton SE, Dayton PA. Optimization of contrast-to-tissue ratio and role of bubble destruction in dual-frequency contrast-specific acoustic angiography imaging. 2014 IEEE Int Ultrason Symp (IUS). 2014b:1774–7.

Ma J, Guo S, Wu D, Geng X, Jiang X. Design, fabrication, and characterization of a single-aperture 1.5-MHz/3-MHz dual-frequency HIFU transducer. IEEE Trans Ultrason Ferroelectr Freq Control. 2013a; 60:1519–29. [PubMed: 25004519]

Ma J, Jiang X, Heath Martin K, Dayton PA. Small aperture, dual frequency ultrasound transducers for intravascular contrast imaging. 2013 IEEE Int Ultrason Symp (IUS). 2013b:769–72.

Ma J, Jiang X, Martin KH, Dayton PA, Li Y, Zhou Q. Dual frequency transducers for intravascular ultrasound super-harmonic imaging and acoustic angiography. 2014 IEEE Int Ultrason Symp (IUS). 2014a:675–8.

Ma J, Li S, Wang Z, Jiang X. Anti-matching design for wave isolation in dual frequency transducer for intravascular super-harmonic imaging. Proc ASME 2014 IMECE. 2014b in press.

Ma J, Martin KH, Dayton PA, Jiang X. A preliminary engineering design of intravascular dual-frequency transducers for contrast enhanced acoustic angiography and molecular imaging. IEEE T Ultrason Ferr. 2014c; 61:870–80.

Ma J, Steer MB, Jiang X. An acoustic filter based on layered structure. Manuscript sumbitted for publication.

Ma J, Wang Z, Jiang X. Design, fabrication, and test of a small aperture, dual frequency ultrasound transducer. Proc SPIE. 2013c; 8695:86951H.

Martin K, Lindsey B, Ma J, Lee M, Li S, Foster F, Jiang X, Dayton P. Dual-Frequency Piezoelectric Transducers for Contrast Enhanced Ultrasound Imaging. Sensors. 2014; 14:20825–42. [PubMed: 25375755]

Naghavi M, Libby P, Falk E, Casscells SW, Litovsky S, Rumberger J, Badimon JJ, Stefanadis C, Moreno P, Pasterkamp G. From vulnerable plaque to vulnerable patient a call for new definitions and risk assessment strategies: part I. Circulation. 2003; 108:1664–72. [PubMed: 14530185]

Neer, PLMJv; Matte, G.; Danilouchkine, MG.; Prins, C.; Adel, Fvd; Jong, Nd. Super-harmonic imaging: development of an interleaved phase-array transducer. IEEE Trans Ultrason Ferroelectr Freq Control. 2010; 57:455–68. [PubMed: 20178912]

Newnham R, Skinner D, Cross L. Connectivity and piezoelectric-pyroelectric composites. Mater Res Bull. 1978; 13:525–36.

Nissen SE, Gurley JC, Grines CL, Booth DC, McClure R, Berk M, Fischer C, DeMaria A. Intravascular ultrasound assessment of lumen size and wall morphology in normal subjects and patients with coronary artery disease. Circulation. 1991; 84:1087–99. [PubMed: 1884441]

Park SE, Shrout TR. Characteristics of relaxor-based piezoelectric single crystals for ultrasonic transducers. IEEE Trans Ultrason Ferroelectr Freq Control. 1997; 44:1140–7.

Qiu W, Chen Y, Wong CM, Liu B, Dai J, Zheng H. A Novel Dual-frequency Imaging Method for Intravascular Ultrasound Applications. Ultrasonics. 2014 in press.

Radhakrishnan K, Bader KB, Haworth KJ, Kopechek JA, Raymond JL, Huang SL, McPherson DD, Holland CK. Relationship between cavitation and loss of echogenicity from ultrasound contrast agents. Phys Med Biol. 2013; 58:6541. [PubMed: 24002637]

Rehrig PW, Hackenberger WS, Jiang X, Shrout TR, Zhang S, Speyer R. Status of piezoelectric single crystal growth for medical transducer applications. 2003 IEEE Int Ultrason Symp (IUS). 2003; 1:766–9.

Shah F, Balan P, Weinberg M, Reddy V, Neems R, Feinstein M, Dainauskas J, Dainauskas J, Meyer P, Goldin M, Feinstein SB. Contrast-enhanced ultrasound imaging of atherosclerotic carotid plaque neovascularization: a new surrogate marker of atherosclerosis? Vasc Med. 2007; 12:291–7. [PubMed: 18048465]

Slager CJ, Wentzel JJ, Schuurbiers JC, Oomen JA, Kloet J, Krams R, Von Birgelen C, Van Der Giessen WJ, Serruys PW, De Feyter PJ. True 3-dimensional reconstruction of coronary arteries in patients by fusion of angiography and IVUS (ANGUS) and its quantitative validation. Circulation. 2000; 102:511–6. [PubMed: 10920062]

Streeter JE, Gessner R, Miles I, Dayton PA. Improving sensitivity in ultrasound molecular imaging by tailoring contrast agent size distribution: in vivo studies. Mol imaging. 2010; 9:87. [PubMed: 20236606]

Szabo, TL. a Diagnostic ultrasound imaging: inside out. Boston: Academic Press; 2014.

Tobis JM, Mallery J, Mahon D, Lehmann K, Zalesky P, Griffith J, Gessert J, Moriuchi M, McRae M, Dwyer ML. Intravascular ultrasound imaging of human coronary arteries in vivo. Analysis of tissue characterizations with comparison to in vitro histological specimens. Circulation. 1991; 83:913–26. [PubMed: 1999040]

Vallabhajosula S, Fuster V. Atherosclerosis: imaging techniques and the evolving role of nuclear medicine. J Nucl Med. 1997; 38:1788–96. [PubMed: 9374357]

Wang JA, Klibanov AL, Mauldin F. Binding dynamics of targeted microbubbles in response to modulated acoustic radiation force. Phys Med Biol. 2014; 59:465–84. [PubMed: 24374866]

Yuan J, Rhee S, Jiang X. 60 MHz PMN-PT based 1-3 composite transducer for IVUS imaging. 2006 IEEE Int Ultrason Symp (IUS). 2008:682–5.

Yuan JR, Jiang X, Cao PJ, Sadaka A, Bautista R, Snook K, Rehrig P. 5C-5 High Frequency Piezo Composites Microfabricated Ultrasound Transducers for Intravascular Imaging. 2006 IEEE Int Ultrason Symp (IUS). 2006:264–8.

Zhang S, Li F, Jiang X, Kim J, Luo J, Geng X. Advantages and Challenges of Relaxor-PbTiCK $_3$ Ferroelectric Crystals for Electroacoustic Transducers-A Review. Prog Mater Sci. 2015; 68:1–66. [PubMed: 25530641]

Zhou S, Hossack JA. Investigation of digital filtering for stacked, phased ultrasound transducers. 2002 IEEE Int Ultrason Symp (IUS). 2002; 2:1201–4.

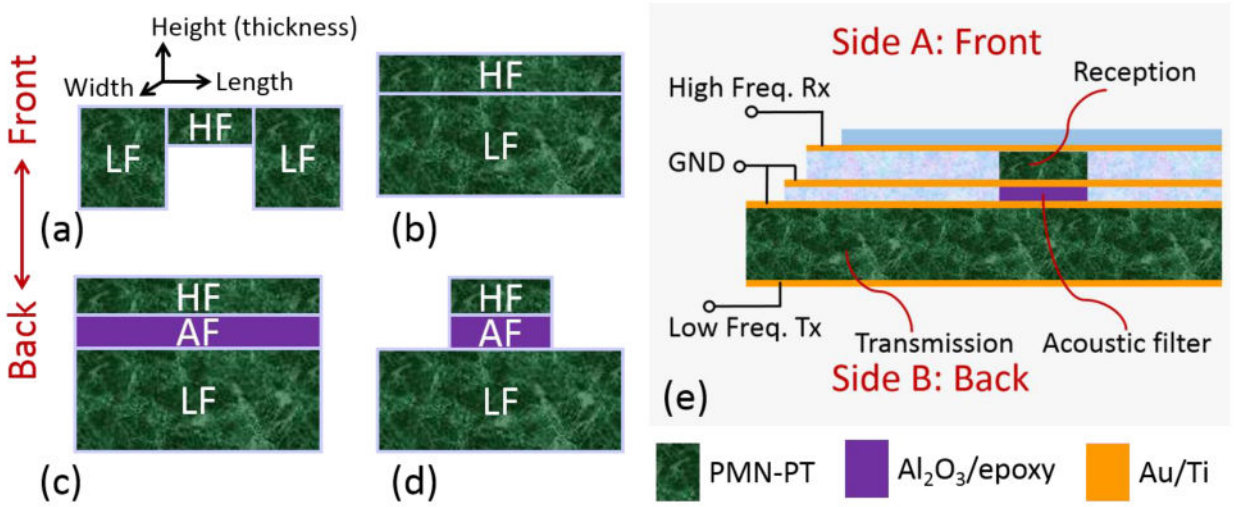

Figure 1.

Side view of the layout design of the dual frequency transducer with: (a) interleaved configuration, (b) stacked configuration, (c) stacked configuration with acoustic filter, (d) stacked configuration with different apertures and acoustic filter, and (e) Final configuration of the transducer including a matching layer and electrical connections. Abbreviations HF, LF and AF denote high frequency, low frequency and acoustic filter, respectively.

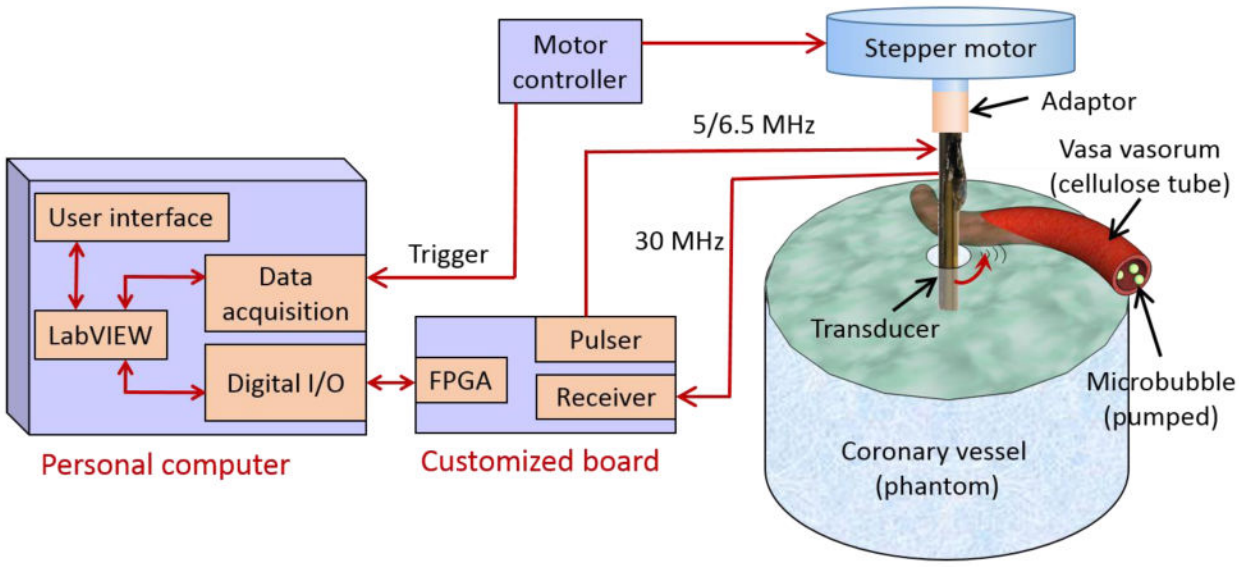

Figure 2.
Cartoon illustrating the setup of the acoustic angiography phantom tested *in vitro*.

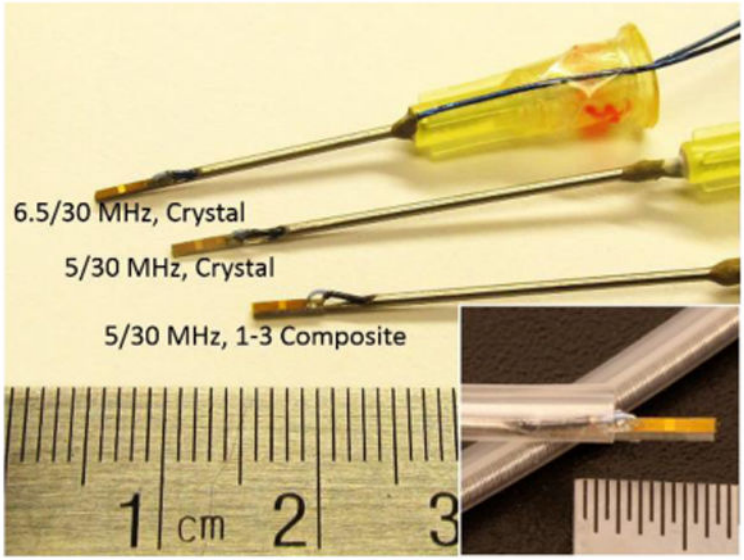

Figure 3.
The transducer prototypes made at different frequencies with different piezoelectric materials. The lower right inset shows the transducer mounted inside a commercial sheathing.

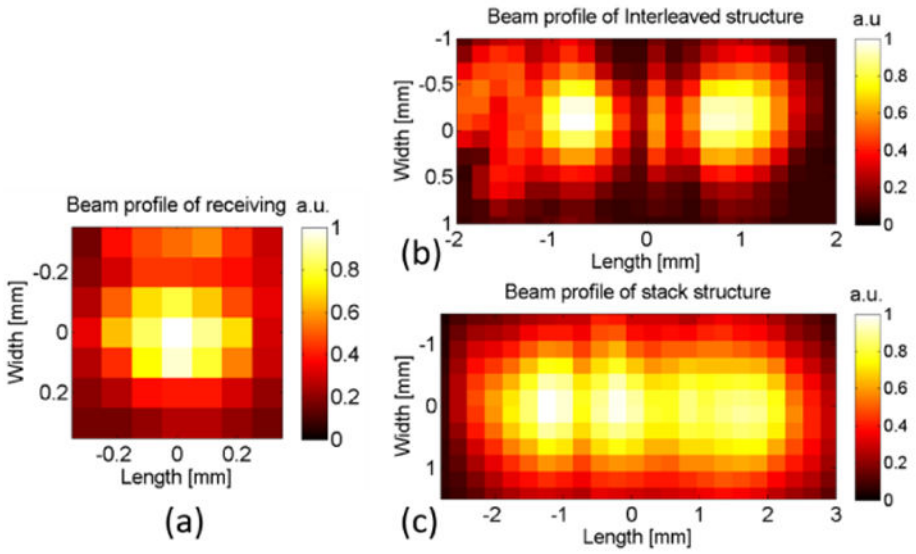

Figure 4.

Beam profile of the (a) receiving beam, and the transmitting beam of (b) the interleaved configuration and (c) the stacked configuration with an acoustic filter.

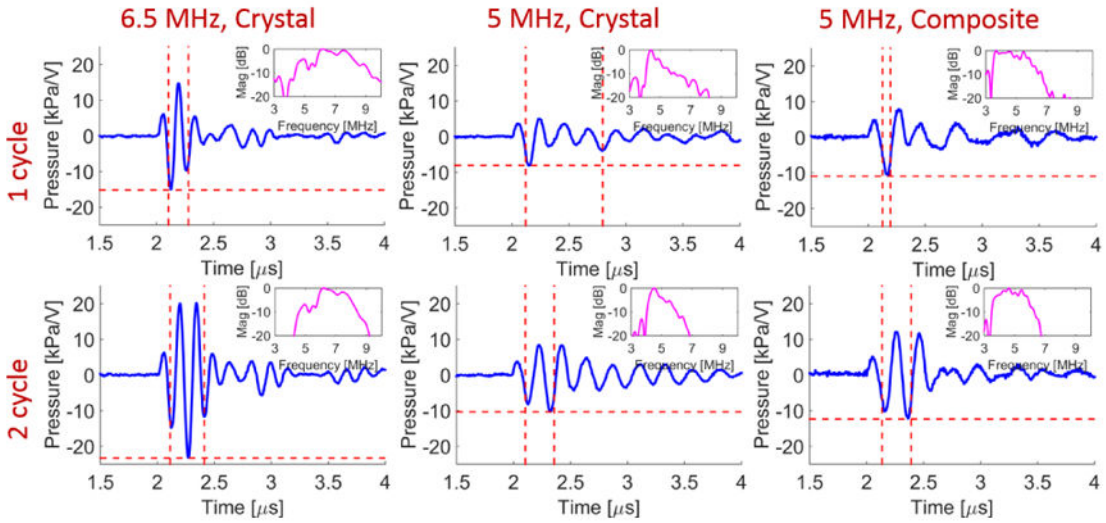

Figure 5.

Transmission efficiency of the prototype transducers for 1 cycle (left) and 2 cycle (right) burst excitation waves. Horizontal lines are drawn to indicate the peak negative pressure of the time series waveform and the vertical lines indicate the -6 dB beginning and end of the pulse for measurement of the pulse length. All values are normalized to input voltage amplitudes

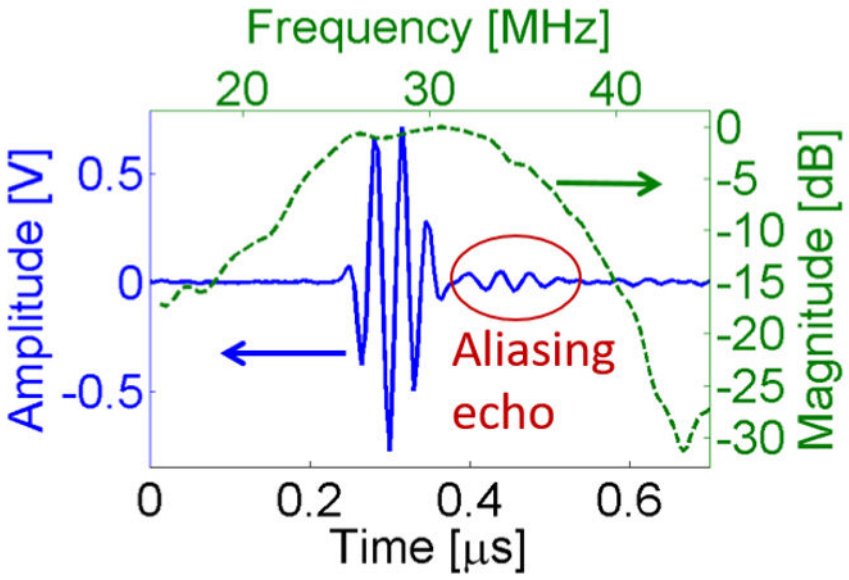

Figure 6.
Pulse-echo response of the 30 MHz reception element.

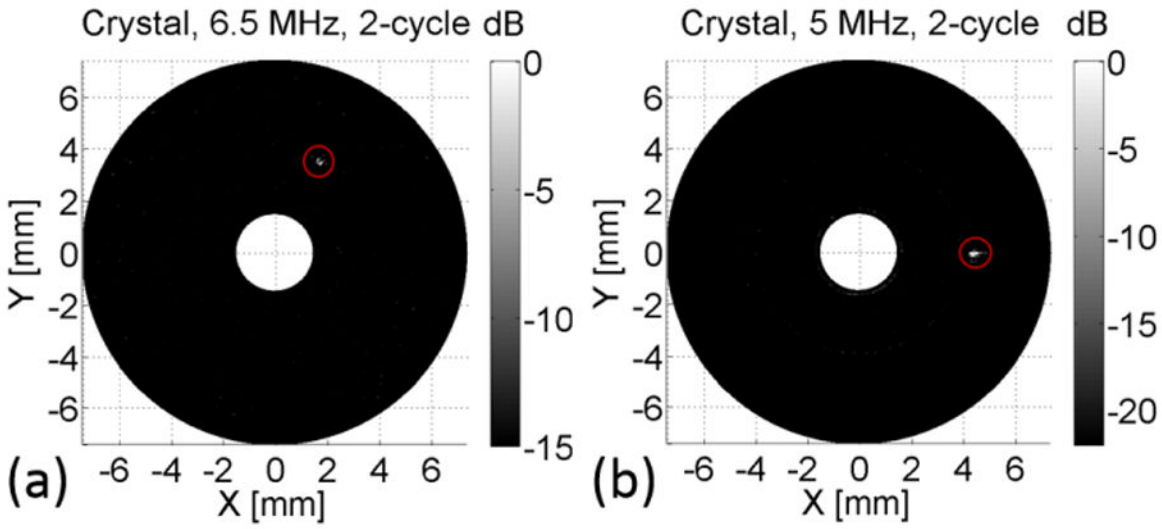

Figure 7.

Comparison of contrast to tissue ratio with excitations at frequencies of (a) 6.5 MHz and (b) 5 MH with 2-cycle excitation.

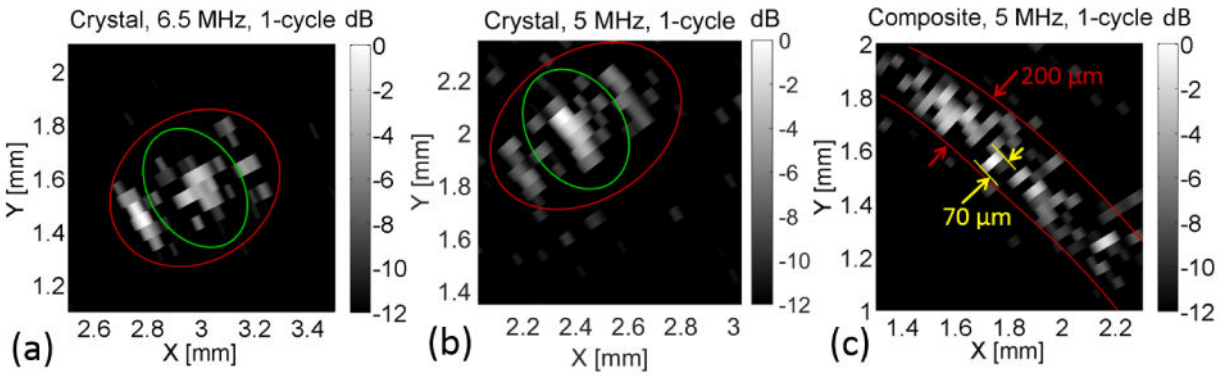

Figure 8.

Comparison of axial resolution with excitations from transducers made of (a) 6.5 MHz PMN-PT single crystal, (b) 5 MHz single crystal and (c) 5 MHz PMN-PT 1-3 composite with 1-cycle excitation.

Table 1

Typical parameters of piezoelectric materials.

Parameters	PZT-5H	PMN-PT	PMN-PT composite
Relative dielectric constant ε_r	3500	8200	4000
Piezoelectric strain/charge constant d_{33} (pC/N)	590	2800	2800
Electromechanical coupling factor k_t	0.5	0.6	> 0.7
Sound speed c (m/s)	4400	4610	3950
Acoustic impedance Z (MRayl)	34	37	18
Curie temperature Tc (°C)	190	155	155
Phase transition temperature T_{rt} (°C)	N/A	65	65

Table 2

Statistical information of the transducer groups.

Transmitter	6.5 MHz single crystal	5 MHz single crystal
Average value (dB)	15.4	21.6
Standard deviation (dB)	1.5	3.0